crystals

MDPI

Article

Disulfide-Modified Mesoporous Silica Nanoparticles for Biomedical Applications

Melissa Venedicto [1], Jake Carrier [2], Ha Na [1], Chen-Yu Chang [1], Daniela R. Radu [1] and Cheng-Yu Lai [1,2,*]

[1] Department of Mechanical and Materials Engineering, Florida International University (FIU), Miami, FL 33174, USA
[2] Department of Chemistry and Biochemistry, Florida International University (FIU), Miami, FL 33174, USA
* Correspondence: clai@fiu.edu

Abstract: Mesoporous silica nanoparticles (MSNs) are highly porous carriers used in drug and gene delivery research for biomedical applications due to their high surface area, narrow particle size distribution, and low toxicity. Incorporating disulfide (SS) bonds into the walls of MSNs (MSN-SSs) offers a dual pathway for drug release due to the pore delivery and collapsing porous structure after cellular engulfment. This study explores the effect of embedding disulfide bonds into MSNs through various structural and biological characterization methods. Raman spectroscopy is employed to detect the SS bonds, SEM and TEM for morphology analyses, and a BET analysis to determine the required amount of SSs for achieving the largest surface area. The MSN-SSs are further loaded with doxorubicin, an anticancer drug, to assess drug release behavior under various pH conditions. The MSN-SS system demonstrated an efficient pH-responsive drug release, with over 65% of doxorubicin released under acidic conditions and over 15% released under neutral conditions. Cleaving the SS bonds using dithiothreitol increased the release to 94% in acidic conditions and 46% in neutral conditions. Biocompatibility studies were conducted using cancer cells to validate the engulfment of the nanoparticle. These results demonstrate that MSN-SS is a feasible nanocarrier for controlled-release drug delivery.

Keywords: mesoporous silica nanoparticles; disulfide bond functionality; controlled-release drug delivery; biomaterials; nanocarriers; cancer research

Citation: Venedicto, M.; Carrier, J.; Na, H.; Chang, C.-Y.; Radu, D.R.; Lai, C.-Y. Disulfide-Modified Mesoporous Silica Nanoparticles for Biomedical Applications. *Crystals* **2023**, *13*, 1067. https://doi.org/10.3390/cryst13071067

Academic Editors: Mohammed Rafi Shaik, Syed Farooq Adil and Mujeeb Khan

Received: 12 June 2023
Revised: 1 July 2023
Accepted: 4 July 2023
Published: 6 July 2023

1. Introduction

Cancer treatments, such as surgery, radiotherapy, and chemotherapy, often impact healthy organs due to the lack of tumor site targeting and drug side effects [1,2]. To increase cancer therapy safety, direct tumor targeting via nanoparticle-based drug-delivery systems (DDSs) is a possible solution [2,3]. The DDS must be designed with the following characteristics: (1) include functional groups that target and anchor on specific tumor receptors; (2) embed a mechanism to avoid triggering an immune response; (3) prevent degradation or any structural changes in the encapsulated drug; and (4) enable encapsulated drug release once the carrier reaches the target site [4,5]. Among various DDSs, mesoporous silica nanoparticles (MSNs) provide a high surface area, narrow pore size distribution, and high pore volume, and they are biocompatible [2,6]. The external surface enhances biocompatibility, as the presence of silanol groups does not pose toxicity when interacting with the phospholipid bilayer of the cell membrane [7]. The MSN external surface could be functionalized by targeting functional groups, including proteins, peptides, or saccharides [8]. Drug delivery was demonstrated both in vitro and in vivo, primarily taking advantage of pores' capacity to upload and release a drug (cargo). The cargo encapsulation mechanisms involved both covalent and non-covalent bonding of the drug with the pore walls, while the surface of the MSN was often functionalized to enhance targeting [9–11].

Herein, we report a novel MSN-based system featuring an alternative drug-release pathway from MSN that involves not only drug release from pores but also nanostructural

pore collapse upon cell entry, thus facilitating fast biodegradation and the elimination of MSN degradation byproducts. In this approach, disulfide bonds are incorporated into the pore walls of MSN during synthesis. The disulfide-modified MSN (MSN-SS) structure was determined using X-ray powder diffraction (XRD), and the surface area of the material was measured using nitrogen physisorption with the Brunauer–Emmett–Teller (BET) method. Transmission electron microscopy (TEM) revealed the MSN characteristic porosity, which was not disrupted or collapsed by the incorporation of disulfide bonds in the MSN walls. The disulfide bond presence was identified using Raman spectroscopy. Scanning electron microscopy (SEM) validated the retention of nanoparticle morphology. Ultraviolet–visible (UV-vis) spectroscopy was used to quantify the MSN-SS drug loading efficiency. The cumulative release of the anticancer drug from the nanocarrier was determined using time-dependent UV-vis absorbance studies, and confocal imaging showed the location of the material in the cells. This study demonstrates that incorporating disulfide bonds in the MSN framework enhances drug delivery efficiency without affecting the material's biocompatibility.

2. Materials and Methods

2.1. Chemicals and Materials

All chemicals employed in this work were used as received without further purification. (1-Hexadecyl)trimethylammonium bromide (CTAB, 98%) was purchased from Alfa Aesar (Tewksbury, MA, USA), bis(3-(triethoxysilyl)propyl)disulfide 90% was purchased from Gelest (Morrisville, PA, USA), ACS-grade methanol from Fisher Chemical (Hampton, NH, USA), tetraethyl orthosilicate (TEOS, 98%) from Alfa Aesar (Tewksbury, MA, USA), sodium hydroxide from J.T.Baker Chemical Company (Phillipsburg, NJ, USA), ACS-reagent-grade nanopure water from Ricca chemical company (Arlington, TX, USA), ACS-grade hydrochloric acid (HCL, 37%) from Acros Organics (Fair Lawn, NJ, USA), and doxorubicin hydrochloride salt (DOX, >99%) from LC Laboratories (Woburn, MA, USA). Cell Counting kit-8 (CCK-8) was purchased from GLPBIO Technology Inc. (Montclair, CA, USA). Gibco Dulbecco's Modified Eagle Medium (DMEM) was bought from Thermo Fisher (Waltham, MA, USA), and Dulbecco's phosphate-buffered saline (DPBS) from Lonza Bioscience (Walkersville, MD, USA). DAPI (4′,6-Diamidino-2-Phenylindole, Dihydrochloride) was purchased from Thermo Fisher (Waltham, MA, USA). HeLa cervical cancer cells were purchased from the Antibody Research Corporation (Saint Charles, MO, USA), and the Green Fluorescence Protein (GFP)-modified human lung carcinoma cell line (A549 GFP) from MyBioSource, Inc. (San Diego, CA, USA).

2.2. Synthesis of Mesoporous Silica Nanoparticle (MSN) Embedded with Disulfide Bonds

MSN was prepared following a literature-modified procedure [12–14]. In a typical experiment, CTAB (2.00 g, 5.48 mmol) was dissolved in nanopure water (480 mL), followed by the addition of NaOH (7 mL of a 2.00 M solution). This mixture was heated under stirring and kept at 85 °C to ensure the complete dissolution of CTAB. Subsequently, 10 mL of the silica precursor was added swiftly to the mixture, which was continuously stirred for two hours. The silica precursors consisted of a mixture of TEOS and bis(triethoxysilylpropyl) disulfide; the latter's concentration varied (Table 1), targeting a material with the highest surface area. The resulting white precipitate was isolated via filtration of the hot suspension. The filtrate was washed three times with nanopure water and twice with methanol. The final product, called hereafter "as-synthesized MSN" (MSN-AS), was dried overnight in a vacuum oven.

Table 1. Amounts of disulfide precursor in each material.

Material Name	Bis(triethoxysilyl-propyl) Disulfide % in the Precursor Mixture
MSN-AS	0%
MSN-AS (5%SS)	5%
MSN-AS (10%SS)	10%
MSN-AS (15%SS)	15%

2.3. CTAB Surfactant Removal from MSN-SS

To remove the surfactant template (CTAB), 1.50 g of MSN-AS was refluxed for 24 h at 75 °C in a methanolic solution of HCl, obtained by mixing 160 mL of methanol with 9 mL of HCl (37%) (18:1 *v*/*v*). The MSN-SSs were collected via filtration. The filtrate was washed three times with nanopure water and twice with methanol, and then it was dried overnight in a vacuum oven. The MSN after wash final product is denoted as MSN-SS.

2.4. Doxorubicin (DOX) Loading

The loading of DOX was conducted over 24 h by mixing 1 mg/mL DOX with a suspension of MSN-SS under constant stirring. In a typical experiment, 10 mg of DOX-hydrochloride was dispersed in 10 mL of nanopure water via ultrasonication for 15 min. Next, 50 mg of MSN-SS was dispersed into 10 mL of nanopure water via ultrasonication for 20 min. Then, 2 mL of the 1 mg/mL DOX was added to a glass vial containing the dispersed MSN-SS mixture and stirred in the dark for 24 h. The mixture was next subjected to centrifugation at 10,000 rpm for 5 min, and the pellet was washed with deionized water three times. The absorbance of each collected supernatant was measured using UV-Vis to determine the DOX concentration and to further calculate the drug loading efficiency (Equation (S1)) [15,16]. After washing, the pellet was freeze-dried for 24 h.

2.5. In Vitro Release of MSN-DOX in Acidic and Neutral pH

A total of 10 mg of MSN-SS-DOX was suspended in 2 mL of pH 5 buffer solution in a glass vial and sonicated to ensure dispersion, followed by stirring in the dark for 48 h. After pre-determined time intervals (1, 2, 4, 6, 8, 24, and 48 h), the dispersion was centrifuged at 10,000 rpm for 5 min. The absorbance of the supernatant was measured using UV-vis at λ_{max} = 480 nm, corresponding to DOX absorbance. After the measurement, the pellet was washed with a buffer, redispersed, and allowed to stir until the next time. This process was repeated for neutral environments using a pH 7.4 buffer. The cumulative release profile for each pH was determined using a calibration curve (Figure S1).

2.6. Dithiothreitol (DTT)-Triggered DOX Release from MSN-SS

The particles were dispersed in the 2.0 mL 10 mM DTT solution prepared in DPBS 1X and placed in culture plates at 37 °C for 48 h. After one hour, the supernatant was removed, and its UV-vis absorbance was measured to determine the amount of released DOX. A fresh medium was added next, and the experiment was repeated for 2, 4, 6, 8, 24, and 48 h. A control experiment was conducted using DPBS 1X without DTT.

2.7. Cytotoxicity of MSN-SS-DOX

HeLa cervical cancer cells were seeded in 96-well plates (7×10^3 cells/well in 250 µL DMEM) and incubated under a 5% CO_2 atmosphere at 37 °C for 24 h. After 24 h, the cells reached 50% confluency, and the media were replaced with a mixture of 25 µL of the MSN-10%SS-DOX aqueous dispersion at different concentrations (0, 0.1, 1, 10, 25, 50, 100, 150, and 200 µg/mL) and 225 µL of fresh media in each well. The treated cells were placed in an incubator for another 24 h. A Cell Counting Kit-8 Assay determined the number of viable cells. In this experiment, the media were replaced with a mixture of 10 µL Cell Counting Kit 8 reagent (CCK-8) and 100 µL fresh media, and cell viability was determined by measuring the absorbance at λ_{max} = 450 nm (characteristic of the formazan

dye generated in viable cells) [17]. This process was repeated for A549 GFP cells. All experiments were performed in four replicates.

2.8. Cellular Uptake of MSN-SS-DOX

HeLa cells were seeded (7.5×10^4 cells/well) in 6-well plates lined with coverslips, in 2 mL of DMEM, and allowed to grow for 24 h. Next, the media were removed, and the cells were treated with 800 µL of MSN-10%SS-DOX prepared as a 200 µg/mL stock. Then, 1.6 mL of fresh media were added to each well to reach a final concentration of 66.7 µg/mL MSN-10%SS-DOX. Experiments were conducted for 2 h, 4 h, 8 h, 24 h, and 48 h periods. Subsequently, the cells were washed with DPBS twice and fixed with 1 mL of 4% formaldehyde in the DPBS buffer for 15 min. After aspirating the fixing agent, the cells were washed three times with DPBS and allowed to absorb the DAPI medium (2.5 µg/mL solution). The cells were washed once with DPBS and once with nanopure water, and the cell-containing coverslips were removed from the wells and placed on a microscope slide for imaging. A fluorescence microscope (EVOS, Invitrogen) was used for imaging. Each experiment was performed in triplicate.

2.9. Characterization

X-ray diffraction (XRD) measurements of MSN-SSs were performed on a RigakuMini-Flex600 (Rigaku, Tokyo, Japan) equipped with a Cu Kα radiation source (λ = 1.5405 Å). The XRD measurements started from 1.5° to 6° with a step size of 0.01° and scan speed of 1°/min. A field-emission scanning electron microscope with energy-dispersive X-ray spectroscopy (SEM-EDS) (JEOL F100, Peabody, MA, USA) was used to determine the morphology of the MSNs. In addition, a transmission electron microscope (TEM) was also used to observe the morphology of the MSNs (JEOL JEM-2100, 200 kV, Peabody, MA, USA). UV-Vis–NIR spectra of the MSN-SSs and the MSN-SS-DOXs were collected utilizing a UV-3600 plus spectrophotometer (Shimadzu, Kyoto, Japan). Raman spectroscopy was performed with a confocal Raman microscope (WITec alpha300 R) using a 532 nm laser. Dynamic light scattering (DLS, Malvern Panaytical, Malvern, United Kingdom) was used to determine the zeta potential of MSN-SS. An inverted multichannel fluorescence microscope (EVOS Imaging M7000) was used to image the cellular uptake of the MSN-SS-DOX. The Brunauer–Emmet–Teller (BET) surface area was determined with a Quantachrome Nova Touch LX2 (Anton Parr, Texas, USA) gas adsorption analyzer using high-purity nitrogen as the adsorbate gas.

3. Results

3.1. Synthesis of MSN-SS

A schematic representation of the MSN-SS synthesis is shown in Figure 1. The MSN synthesis procedure used bis(triethoxysilyl-propyl) disulfide (Figure 2c) in conjunction with TEOS as silica precursors to obtain the MSN-SS materials. The presence of disulfide bonds in the final product was validated using Raman spectroscopy.

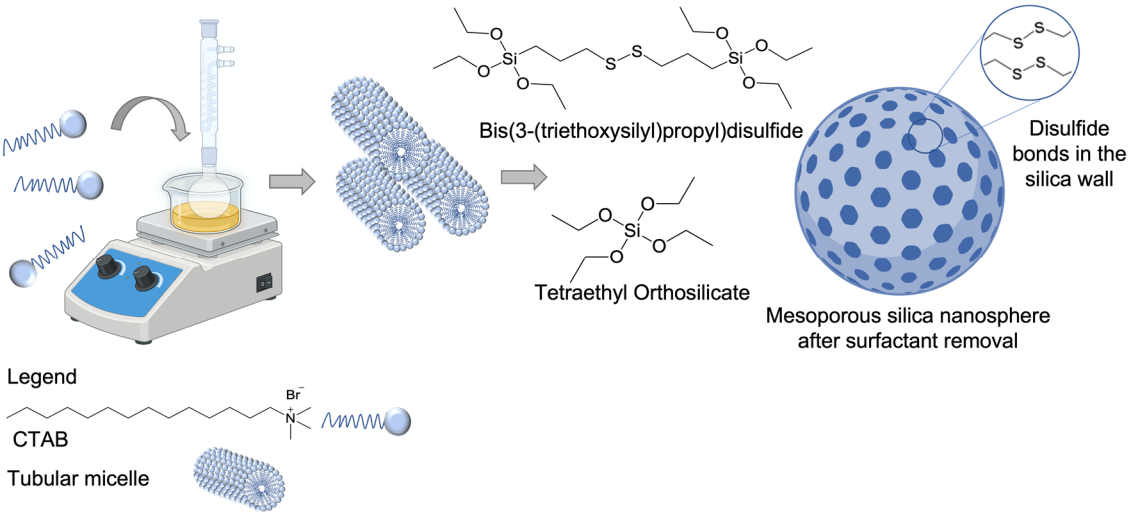

Figure 1. As-synthesized MSN-SS-AS reaction scheme, formation of the surfactant micelle from CTAB precursor in nanopure water in basic pH. Upon addition of TEOS and disulfide silane precursor, the micelles MSN is formed, with some of the disulfide precursor is entrapped inside the pores.

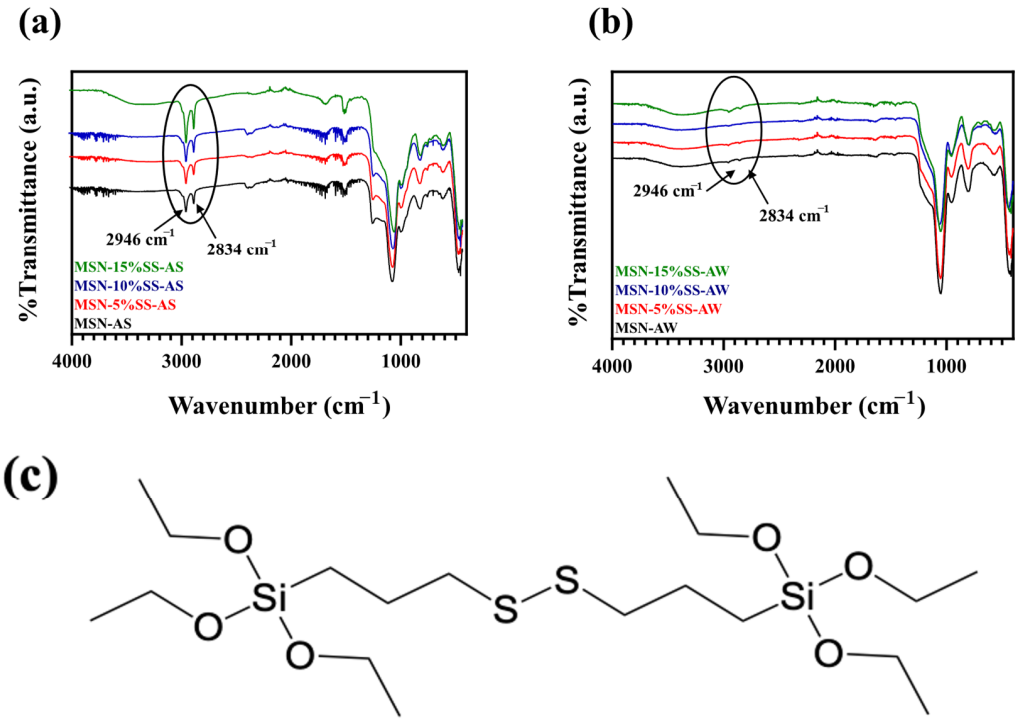

Figure 2. FTIR of (**a**) as-synthesized MSN-AS with the CTAB surfactant and disulfide inside the pores for different concentrations of disulfide precursor, and (**b**) after wash (MSN-SS) for different concentrations of disulfide precursor. (**c**) Molecular structure of bis(3-(triethoxysilyl)propyl) disulfide.

3.2. Infrared Spectroscopy—MSN and Surface Modifications

FTIR was used to confirm the removal of CTAB during the methanolic HCl wash. The IR spectra in Figure 2a,b suggest the removal of CTAB due to the significant decrease in the CTAB alkyl chain characteristic peaks (C-H stretching) at 2946 cm^{-1} and ~2834 cm^{-1}, respectively [18].

3.3. Raman Analysis of MSN-SS

The Raman spectra of the as-synthesized MSN-SS samples displayed disulfide peaks at 508 cm^{-1} (Figure 3a), which agrees with previous reports [19]. The peak around 759 cm^{-1} indicates the presence of the CTAB surfactant in Figure 2a [20]. The MSN framework appears at 632 cm^{-1} in both Figures 3a and 3b [21].

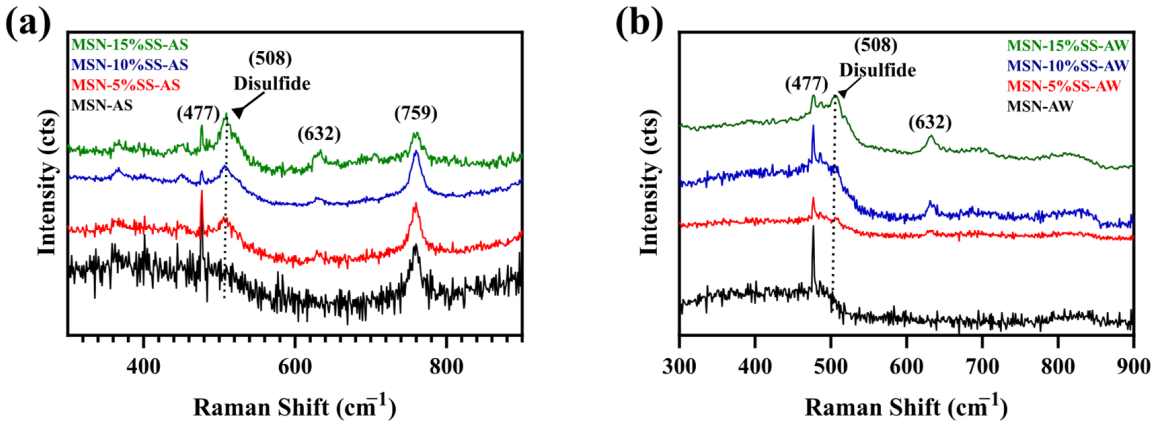

Figure 3. Raman spectra of materials for different concentrations of disulfide precursor: (**a**) As-synthesized MSN-SS (MSN-AS) with the CTAB surfactant and disulfide inside the pores and (**b**) after wash (MSN-SS).

3.4. BET Analysis of MSN-SS

The MSN-AS and MSN-SS were characterized using nitrogen physisorption to identify the variant with the highest surface area. The specific surface area of the nanoparticles was measured using the Brunauer–Emmett–Teller (BET) method, and the pore size distribution was determined using the density functional theory (DFT) method. All samples were degassed for 16 h at 100 °C to ensure the adequate removal of surface adsorbed moisture prior to analysis. Measurements were performed at 77.35 K in the relative pressure range of 0.005–0.995 P/P_0 with a tolerance of ± 0.05 P/P_0 and an equilibration time of 60 s. All silica nanoparticles displayed a Type IV isotherm with a peak at approximately 0.3 P/P_0, characteristic of mesoporous materials, and a high surface area of 1228.774 m^2/g, as shown in Figure 4. The surface area and pore size are summarized in Table 2, indicating that the largest surface area was obtained using a 10% disulfide precursor. Therefore, MSN-10%SS was selected for further experiments in this work.

Table 2. BET surface area and DFT pore size of the MSN-SSs.

Material	Surface Area (m^2/g)	Pore Width (nm)
MSN-SS	1106.674	4.08
MSN-SS 5%	1149.435	2.88
MSN-SS 10%	1228.774	2.86
MSN-SS 15%	1029.973	3.52

The diffraction patterns for MSN-SS-AS and MSN-SS-AW are shown in Figure 5. The XRD shows the characteristic peaks of mesoporous silica materials, with a strong peak at 2.55°, corresponding to the (100) plane, and diffraction peaks at 3.9° and 4.2°, representing the (110, 200) planes [22]. Comparing the diffraction peaks between MSN-AS and MSN-SS, the peaks for MSN-AS have a lower intensity due to the presence of CTAB inside the pores (Figure 6a) and have an increase in 2θ in the absence of the surfactant in MSN-AW (Figure 6b).

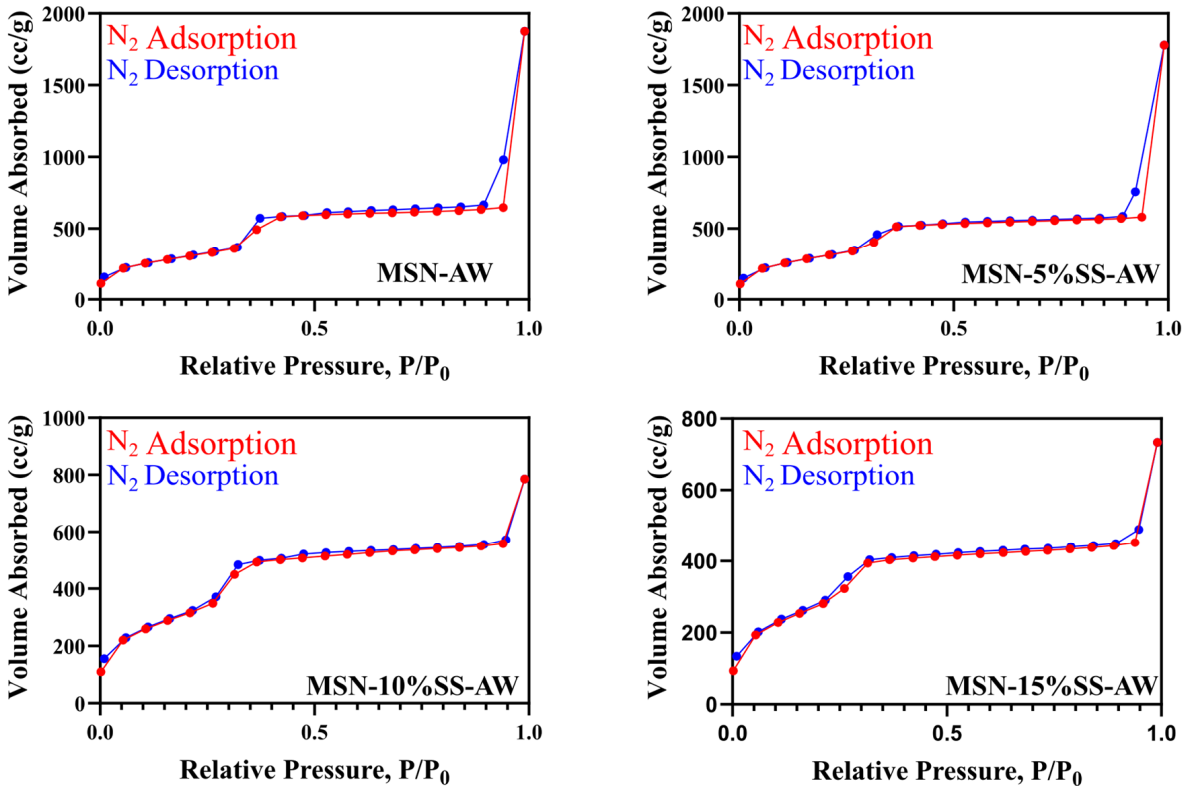

Figure 4. BET Analysis—nitrogen adsorption–desorption isotherms measured at 77.35 K.

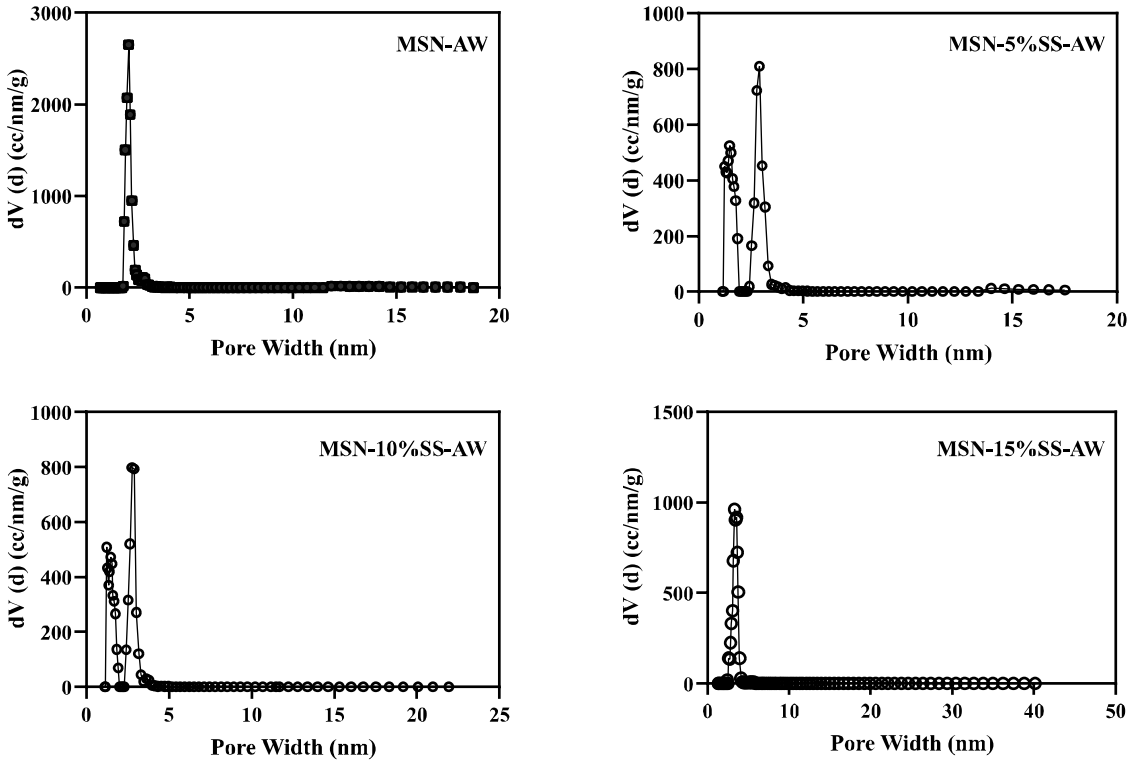

Figure 5. Pore size and distribution analysis of MSN-SS nanocarriers via DFT method.

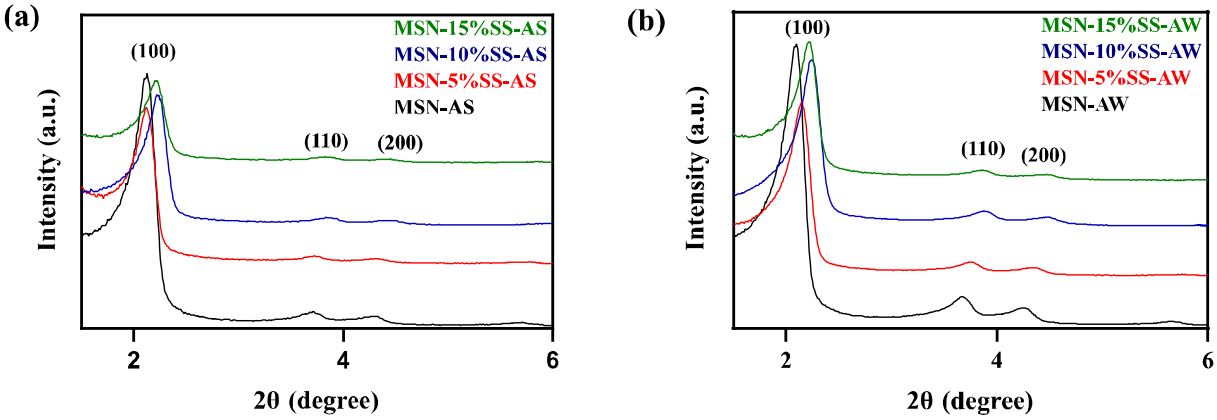

Figure 6. XRD analysis of MSN-SSs: (**a**) as-synthesized and (**b**) after wash.

3.5. Surface Morphology

TEM (Figures 7a and S2) and SEM (Figures 7b and S3) imaging confirmed the retention of parallel pores and the honeycomb pore arrangement in MSN-SS. In addition, TEM also confirmed that including disulfide bonds did not disrupt the pores in the MSN (Figures 7a and S2). These results are consistent with those in the literature, proving the synthesis of the reported MSN [10,12,23].

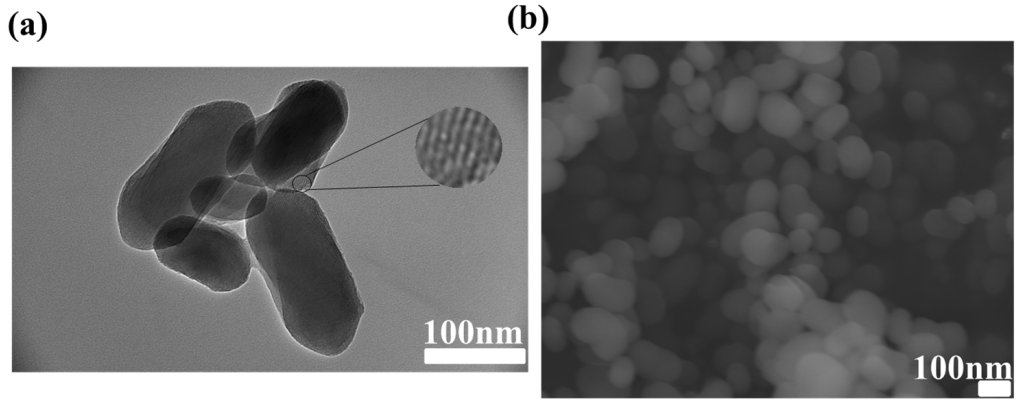

Figure 7. MSN-SS morphology: (**a**) TEM image, (**b**) SEM image.

The zeta potential measurements of the MSN nanocarriers resulted in a less negative zeta potential in the disulfide-modified MSN than in the pure MSN. In the pure MSN, the zeta potential was -20.8 ± 11.8 mV; there was a slight decrease with 5% disulfide bonds (-23.6 ± 13.4 mV) and a jump to $-16. \pm 14.4$ mV for 15% disulfide bonds, suggesting that the presence of disulfide bonds impacted the net charge of the particle (Table S1). The pore size of MSN-SS was approximated using Bragg's Law (Equation (S2)). Notably, the pore size was drastically reduced after doxorubicin loading (Table S3). The effect of pore filling on the MSN-SS pores was consistent with that reported in the literature [24].

3.6. Drug Loading

The maximum loading efficiency amount was shown in the 10% disulfide sample, with a 39.82% loading efficiency (Table 3). The results from the BET analysis after loading with DOX showed a transition from a Type IV isotherm to an isotherm with Type II, typical of non-porous or macroporous material (Figure 8a). An analysis of the pore volume using the DFT method showed a significant decrease in the pore volume from 0.8120 cc/g prior to loading and 0.3630 cc/g after loading. In addition, the MSN-10%SS-AW diffraction lattice parameters, analyzed through the Bragg's Law approximation, decreased after the

incorporation of DOX, further evidencing the successful incorporation of DOX into the MSN pores (Figure S4a and Equation (S2)) [25].

Table 3. The drug loading efficiency of DOX into MSN-SS silica network.

Nanocarrier	Supernatant Concentration (mM)	Amount Loaded (mM)	Loading Efficiency (%)
MSN-AW	0.66888	1.33	30.89
MSN-5%SS	0.55116	1.45	33.61
MSN-10%SS	0.28367	1.72	39.82
MSN-15%SS	1.22714	0.773	17.93

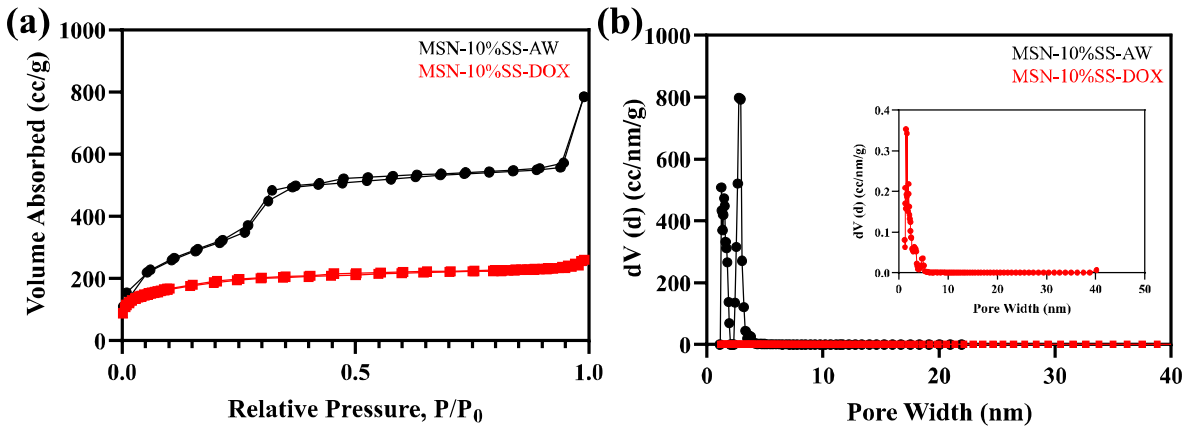

Figure 8. BET analysis of MSN-SS with and without DOX: (**a**) isotherm comparison and (**b**) pore size distribution of MSN-SS with and without DOX, inset contains the pore size distribution of DOX showing presence of macropores.

3.7. In Vitro DOX Release Profiles from MSN Silica Framework

The DOX release was measured using UV-vis spectroscopy at different time intervals (0, 1, 2, 4, 6, 8, 24, and 48 h) at λ_{max} = 480 nm corresponding to DOX absorbance. Three experiments were conducted to (1) investigate DOX release under varying pH conditions, (2) determine the importance of DTT in the release of DOX from MSN-SS, and (3) evaluate the DOX release with DTT under varying pH conditions. We examined the DOX release under different pH conditions, in conjunction with DTT as a reducing reagent that "cleaves" the disulfide bonds. These experiments simulated the in vitro model for future in vivo studies and how the MSN-SS structure would react inside the body. The results show that, at pH 7.4, only a small amount of DOX was released (15%) after 48 h of vigorous stirring at 37 °C. At pH 5, the protonation of the silanol groups on the silica surface led to an increased (65%) DOX release. A second experiment was conducted to determine the significance of DTT for DOX release; MSN-10%SS-DOX was loaded into a suspension of 10 mM DTT. After 48 h, the release of DOX was notably higher in the presence of DTT than in the control group without DTT (Figure 9a). At pH 5 and in the presence of DTT, 94% of DOX was released in 48 h. This is consistent with literature reports where the gradual cleavage of disulfide bonds was demonstrated for solid silica synthetically modified with disulfide bonds [24].

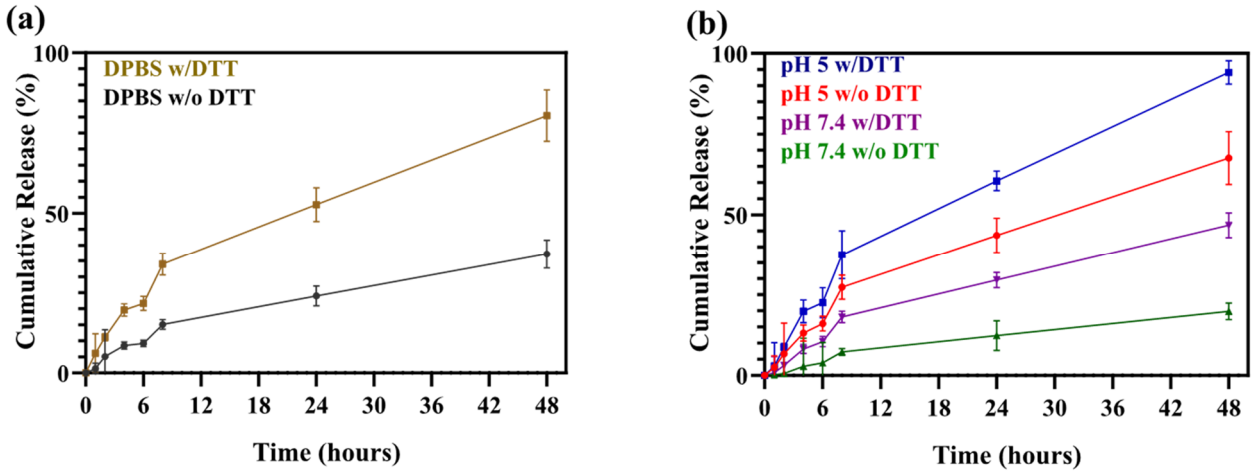

Figure 9. (**a**) Cumulative release profiles of MSN-10%SS-DOX under a DTT study and (**b**) cumulative release profile under two pH conditions and comparison of DTT environments.

3.8. In Vitro Cytotoxicity

The cell viabilities of MSN-10%SS-AW, MSN-10%SS-DOX, and pure DOX on HeLa and endothelial lung cancer cells (A549-GFP) lines were evaluated using a CCK-8 assay. The cancer cells were subjected to various concentrations of MSN-10%SS, such as (0, 0.1, 1, 10, 25, 50, 100, 150, and 200 µg/mL), and they were incubated over 24 h. The results show high biocompatibility among both cell lines, with a cell viability of over 90%, further demonstrating that the surfactant (CTAB) was adequately washed away and did not cause any damage to the cellular membrane [14,26]. In addition, the cytotoxicity study of MSN-10%SS-DOX was conducted using the same parameters and showed a decreasing cell viability as the concentration of the loaded nanoparticles increased (Figure 10). The half-maximum inhibitory concentration (IC50) was calculated to determine the nanoparticles' efficacy in drug delivery [27]. The IC50 for MSN-10%SS-DOX was 15.07 µg/mL in HeLa cells and 12.48 µg/mL in A549-GFP cells. The cytotoxicity of doxorubicin was established as a control experiment, given that the anticancer drug is known to be toxic at low concentrations and to ensure the controllability of the nanoparticle. In the case of the drug alone, the IC50 was calculated to be 9.12 µg/mL in HeLa cells and 8.84 µg/mL in A549-GFP cells. A CCK8 assay is essential for determining DOX toxicity [28,29]. The MSN-SS nanocarrier allows for a tunable release due to the gradual reduction of the disulfide bonds within the silica framework in the cellular environment [30].

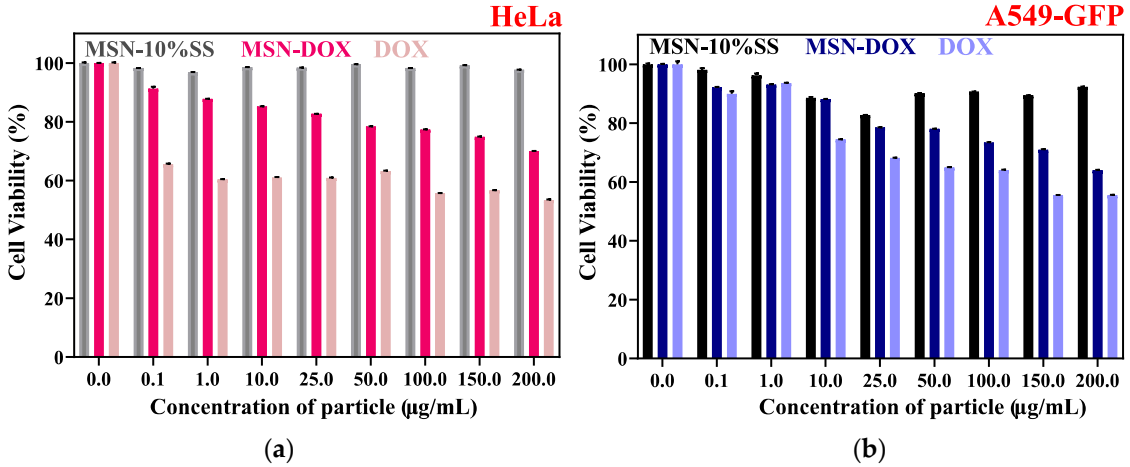

Figure 10. Cytotoxicity study of MSN-10%SS, MSN- 10%SS-DOX, and pure DOX using cancer cell lines HeLa (**a**) and A549-GFP (**b**).

3.9. Cellular Uptake

To verify that the doxorubicin was released from MSN-10%SS into the cancer cells, the nanocarrier was incubated in the HeLa and A549-GFP cells over 48 h. DOX is a fluorescent molecule, enabling imaging of the MSN-10%SS-DOX uptake by cells via fluorescence microscopy. DAPI was used as cell nuclei staining (Figure 11). The composite image of the three channels enables a visualization of the material location in cells. The GFP expressed in the A549-GFP cells was monitored in the green channel, and the intensity of the doxorubicin release over time and its uptake in the cell nuclei were monitored in the red channel. The results indicate that, as the incubation time increased, the cancer cells actively absorbed the MSN-SSs. Additionally, the pH shift from the DMEM medium to the cancer cells' internal environment, which contained other reducing reagents, enabled the release of DOX. These findings align with previous literature reports [31,32]. However, in our case, the DOX release was enhanced by the redox reaction that cleaves the disulfide bonds. The internalized signal increased considerably from 4 to 48 h in both cell lines, with the highest concentration of DOX in the cells at 48 h. Therefore, the fluorescence imaging visualized the uptake of DOX within the nucleus of the cell and proved the results of the biocompatibility studies.

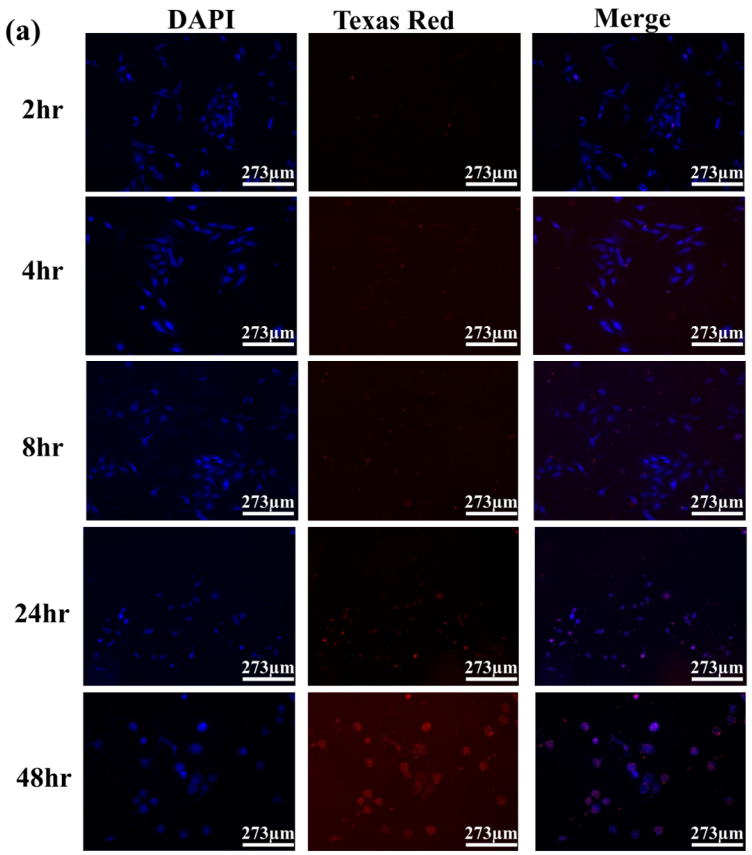

Figure 11. *Cont.*

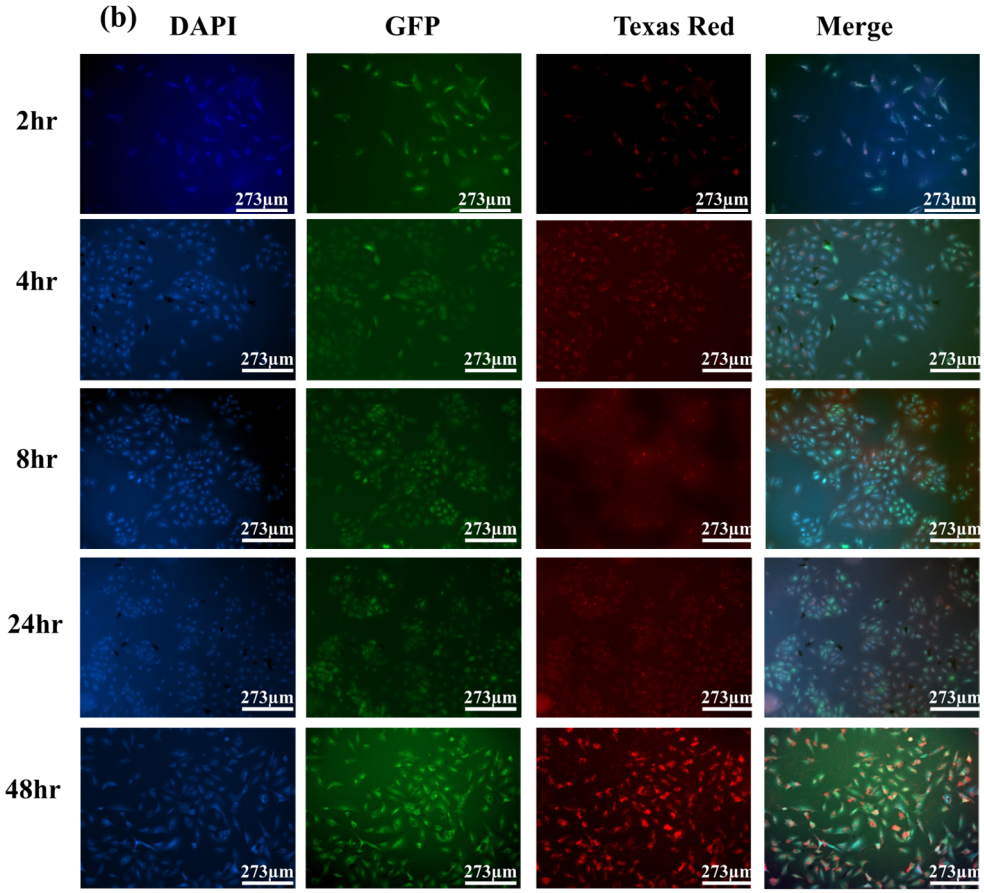

Figure 11. Confocal microscopy imaging MSN--10%SS-DOX-treated cells: (**a**) HeLa cells and (**b**) A549-GFP cells.

4. Discussion

The successful synthesis of MSN-SSs was validated through characterization techniques, such as FTIR, Raman, XRD, BET-DFT, SEM, and TEM. The removal of the CTAB surfactant via methanol washing was evident through the almost complete disappearance of its characteristic peaks in both FTIR and the Raman analysis, as shown in Figures 2b and 3b. This CTAB removal step is critical as it has been previously demonstrated that CTAB is toxic to cells, potentially damaging the cell membrane and causing the release of intracellular enzymes [7]. This step is vital for cellular study, as CTAB has been shown to have toxic effects on cells due to the chances of damaging the cell membrane and inducing a release of intracellular enzymes. While the intensity of the Raman spectra of the disulfide peak decreased after methanol washing (Figure 3b), the peak was still present, suggesting that (1) the use of a methanol acid wash does not disrupt the disulfide bonds within the sample and (2) the synthesis was successful in introducing disulfide bonds in the pore walls.

The pore size analysis was utilized based on the BET-DFT and XRD studies. The BET-DFT analysis revealed that MSN-10%SS presented the largest surface area. The results indicate that, following DOX loading, a significant decrease in the specific surface area from 1228.774 to 676.244 m^2/g occurred (Figure 8a). Incorporating DOX into the pores of the MSN contributed to the decrease in the surface area due to pore filling.

Importantly, the fabrication of the material with the S-S bonds embedded in the pore walls did not alter the typical morphology and porosity of the material, as evidenced by the TEM images, which show parallel pores.

The choice of MSN-10%SS was further evaluated during the drug loading experiments, as this disulfide concentration presented the highest loading capacity. The amount of drug in the nanoparticle was determined using UV-Vis and Equation (S2) (Table 3) [33]. The

in vitro drug release studies were conducted to establish the DOX drug release profile used for cellular studies. The specific pH conditions were selected to validate the release in cancer cell environments, given the acidic nature of the cancer cell. At pH 5, the protonation of the silanol groups within the MSN-SS enabled DOX release from the pores; the use of DTT cleaved the disulfide bonds and allowed for a more significant release of DOX. At pH 7, a neutral environment, the drug release was significantly lower given the lack of protonation of the silanol groups, proving the synergistic effect of DTT and acidic pH. This study demonstrates that the release of the anticancer drug depends on the environment's pH and the presence of reducing reagents.

Cell studies were conducted on HeLa and A549-GFP cancer cells lines to assess the new MSN-SS cytotoxicity and qualitatively observe the drug delivery. The cells were incubated with various concentrations of MSN-10%SS-DOX and pure doxorubicin, and the IC50 was determined.

5. Conclusions

This study demonstrates the usefulness of disulfide-bond-embedded walls in enhancing the drug delivery ability of MSN. Three variants of MSN-SS were fabricated using a mixture of TEOS with a disulfide bond containing silane at 5%, 10%, or 15% as the silica precursor. The material with the largest surface area and highest doxorubicin loading capacity was found to be 10% (MSN-10%SS-DOX), and this was selected for the drug delivery evaluation. UV-VIS was used to determine the drug loading capacity of MSN-SS as 39.8%. An in vitro toxicity study using HeLa and A549-GFP cells demonstrated the biocompatibility of the MSN-SS material (MSN-10%SS) and the ability to release doxorubicin, materialized by cancer cell killing. A confocal imaging time study was employed to visualize the loaded nanoparticles' uptake in the cells and showed that, within 48 h, the drug was released and localized in the nucleus. The tuning of the MSN drug delivery capability by using disulfide bonds proved feasible for the further use of this nanocarrier for controlled-release drug delivery.

Supplementary Materials: The following supporting information can be downloaded at https://www.mdpi.com/article/10.3390/cryst13071067/s1, Figure S1: Doxorubicin calibration curve at 480 nm wavelength; Figure S2: TEM Surface Morphology Comparison of MSN-disulfide; Figure S3: SEM Surface Morphology Comparison of MSN-disulfide; Figure S4: Zeta potential Comparison of MSN-AW to disulfide-MSN; Table S1: MSN zeta potential among various disulfide concentrations; Table S2: MSN-AS nanocarrier using lattice parameter analysis via XRD; Table S3: MSN-AW nanocarrier using lattice parameter analysis via XRD; Figure S5: (a) XRD analysis between MSN-AS, MSN-AW, MSN-DOX, and MSN-DOX-DTT to show deformed structure after pore filling, and (b) FTIR analysis between MSN-AS, MSN-AW, MSN-DOX, and MSN-DOX-DTT.

Author Contributions: Conceptualization, M.V. and C.-Y.L.; methodology, M.V., H.N., D.R.R. and C.-Y.L.; validation, M.V., C.-Y.L., D.R.R., J.C. and C.-Y.C.; formal analysis, M.V., C.-Y.L., D.R.R., J.C. and C.-Y.C.; investigation, M.V., H.N., J.C. and C.-Y.C.; resources, C.-Y.L. and D.R.R.; data curation, M.V., C.-Y.L., D.R.R., J.C. and C.-Y.C.; writing—original draft preparation, M.V.; writing—review and editing, M.V., C.-Y.L. and D.R.R. supervision, C.-Y.L. and D.R.R.; project administration, C.-Y.L. and D.R.R.; funding acquisition, C.-Y.L. and D.R.R. All authors have read and agreed to the published version of the manuscript.

Funding: This research was funded by NASA under grant number 80NSSC19M0201 and grant number 80NSSC22M0134 and in part by the National Science Foundation under grant numbers DMR-2122078, and CBET-1924412. Melissa Venedicto was funded by FIU University Graduate School Presidential Fellowship, and Jake Carrier was funded by FIU University Graduate School Veteran Fellowship.

Data Availability Statement: Data are available from the authors upon reasonable request.

Conflicts of Interest: The authors declare no conflict of interest. The funders had no role in the design of the study; in the collection, analyses, or interpretation of the data; in the writing of the manuscript; or in the decision to publish the results.

References

1. Zhao, D.; Zhang, H.; Yang, S.; He, W.; Luan, Y. Redox-sensitive mPEG-SS-PTX/TPGS mixed micelles: An efficient drug delivery system for overcoming multidrug resistance. *Int. J. Pharm.* **2016**, *515*, 281–292. [CrossRef] [PubMed]
2. Khan, M.I.; Hossain, M.I.; Hossain, M.K.; Rubel, M.H.K.; Hossain, K.M.; Mahfuz, A.M.U.B.; Anik, M.I. Recent Progress in Nanostructured Smart Drug Delivery Systems for Cancer Therapy: A Review. *ACS Appl. Bio Mater.* **2022**, *5*, 971–1012. [CrossRef] [PubMed]
3. Yan, J.; Xu, X.; Zhou, J.; Liu, C.; Zhang, L.; Wang, D.; Yang, F.; Zhang, H. Fabrication of a pH/Redox-Triggered Mesoporous Silica-Based Nanoparticle with Microfluidics for Anticancer Drugs Doxorubicin and Paclitaxel Codelivery. *ACS Appl. Bio Mater.* **2020**, *3*, 1216–1225. [CrossRef] [PubMed]
4. Sharif, F.; Porta, F.; Meijer, A.H.; Kros, A.; Richardson, M.K. Mesoporous silica nanoparticles as a compound delivery system in zebrafish embryos. *Int. J. Nanomed.* **2012**, *7*, 1875–1890. [CrossRef]
5. Jain, V.; Jain, S.; Fau-Mahajan, S.C.; Mahajan, S.C. Nanomedicines based drug delivery systems for anti-cancer targeting and treatment. *Curr. Drug Deliv.* **2015**, *12*, 177–191. [CrossRef]
6. Nairi, V.; Medda, S.; Piludu, M.; Casula, M.; Vallet-Regì, M.; Monduzzi, M.; Salis, A. Interaction between bovine serum albumin and mesoporous silica nanoparticles functionalized with biopolymers. *Chem. Eng. J.* **2018**, *340*, 42–50. [CrossRef]
7. Karimi, M.; Mirshekari, H.; Aliakbari, M.; Sahandi, P.; Hamblin, M. Smart mesoporous silica nanoparticles for controlled-release drug delivery. *Nanotechnol. Rev.* **2015**, *5*, 195–207. [CrossRef]
8. Wang, J.; Li, Y.; Nie, G. Multifunctional biomolecule nanostructures for cancer therapy. *Nat. Rev. Mater.* **2021**, *6*, 766–783. [CrossRef]
9. Rasool, N.; Negi, D.; Singh, Y. Thiol-Functionalized, Antioxidant, and Osteogenic Mesoporous Silica Nanoparticles for Osteoporosis. *ACS Biomater. Sci. Eng.* **2023**, *9*, 3535–3545. [CrossRef]
10. Radu, D.R.; Lai, C.-Y.; Jeftinija, K.; Rowe, E.W.; Jeftinija, S.; Lin, V.S.Y. A Polyamidoamine Dendrimer-Capped Mesoporous Silica Nanosphere-Based Gene Transfection Reagent. *J. Am. Chem. Soc.* **2004**, *126*, 13216–13217. [CrossRef]
11. Castillo, R.R.; Lozano, D.; González, B.; Manzano, M.; Izquierdo-Barba, I.; Vallet-Regí, M. Advances in mesoporous silica nanoparticles for targeted stimuli-responsive drug delivery: An update. *Expert Opin. Drug Deliv.* **2019**, *16*, 415–439. [CrossRef]
12. Na, H.; Venedicto, M.; Chang, C.Y.; Carrier, J.; Lai, C.Y. Infrared-Activated Bactericide: Rhenium Disulfide (ReS(2))-Functionalized Mesoporous Silica Nanoparticles. *ACS Appl. Bio Mater.* **2023**, *6*, 1577–1585. [CrossRef]
13. Lai, C.-Y.; Trewyn, B.G.; Jeftinija, D.M.; Jeftinija, K.; Xu, S.; Jeftinija, S.; Lin, V.S.Y. A Mesoporous Silica Nanosphere-Based Carrier System with Chemically Removable CdS Nanoparticle Caps for Stimuli-Responsive Controlled Release of Neurotransmitters and Drug Molecules. *J. Am. Chem. Soc.* **2003**, *125*, 4451–4459. [CrossRef]
14. Lin, Y.-S.; Haynes, C.L. Impacts of Mesoporous Silica Nanoparticle Size, Pore Ordering, and Pore Integrity on Hemolytic Activity. *J. Am. Chem. Soc.* **2010**, *132*, 4834–4842. [CrossRef]
15. Mao, C.; Xiang, Y.; Liu, X.; Cui, Z.; Yang, X.; Li, Z.; Zhu, S.; Zheng, Y.; Yeung, K.W.K.; Wu, S. Repeatable Photodynamic Therapy with Triggered Signaling Pathways of Fibroblast Cell Proliferation and Differentiation To Promote Bacteria-Accompanied Wound Healing. *ACS Nano* **2018**, *12*, 1747–1759. [CrossRef]
16. Liu, M.; Radu, D.R.; Selopal, G.S.; Bachu, S.; Lai, C.Y. Stand-Alone CuFeSe(2) (Eskebornite) Nanosheets for Photothermal Cancer Therapy. *Nanomaterials* **2021**, *11*, 2008. [CrossRef]
17. Ye, H.; Zhang, Y.; Wang, Y.; Xia, J.; Mao, X.; Yu, X. The restraining effect of baicalein and U0126 on human cervical cancer cell line HeLa. *Mol. Med. Rep.* **2017**, *16*, 957–963. [CrossRef]
18. Shettigar, R.R.; Misra, N.M.; Patel, K. Cationic surfactant (CTAB) a multipurpose additive in polymer-based drilling fluids. *J. Pet. Explor. Prod. Technol.* **2018**, *8*, 597–606. [CrossRef]
19. Mekaru, H.; Yoshigoe, A.; Nakamura, M.; Doura, T.; Tamanoi, F. Biodegradability of Disulfide-Organosilica Nanoparticles Evaluated by Soft X-ray Photoelectron Spectroscopy: Cancer Therapy Implications. *ACS Appl. Nano Mater.* **2018**, *2*, 479–488. [CrossRef]
20. Gao, Y.; Li, L.; Zhang, X.; Wang, X.; Ji, W.; Zhao, J.; Ozaki, Y. CTAB-triggered Ag aggregates for reproducible SERS analysis of urinary polycyclic aromatic hydrocarbon metabolites. *Chem. Commun.* **2019**, *55*, 2146–2149. [CrossRef]
21. Laird, M.; Matsumoto, K.; Higashi, Y.; Komatsu, A.; Raitano, A.; Morrison, K.; Suzuki, M.; Tamanoi, F. Organosilica nanoparticles containing sodium borocaptate (BSH) provide new prospects for boron neutron capture therapy (BNCT): Efficient cellular uptake and enhanced BNCT efficacy. *Nanoscale Adv.* **2023**, *5*, 2537–2546. [CrossRef] [PubMed]
22. Wagner, M.; Krieger, A.; Minameyer, M.; Hämisch, B.; Huber, K.; Drewello, T.; Gröhn, F. Multiresponsive Polymer Nanoparticles Based on Disulfide Bonds. *Macromolecules* **2021**, *54*, 2899–2911. [CrossRef]
23. Akbarian, M.; Gholinejad, M.; Mohammadi-Samani, S.; Farjadian, F. Theranostic mesoporous silica nanoparticles made of multi-nuclear gold or carbon quantum dots particles serving as pH responsive drug delivery system. *Microporous Mesoporous Mater.* **2022**, *329*, 111512. [CrossRef]
24. Du, X.; Kleitz, F.; Li, X.; Huang, H.; Zhang, X.; Qiao, S.-Z. Disulfide-Bridged Organosilica Frameworks: Designed, Synthesis, Redox-Triggered Biodegradation, and Nanobiomedical Applications. *Adv. Funct. Mater.* **2018**, *28*, 1707325. [CrossRef]
25. Jaroniec, M.; Kruk, M.; Shin, H.J.; Ryoo, R.; Sakamoto, Y.; Terasaki, O. Comprehensive characterization of highly ordered MCM-41 silicas using nitrogen adsorption, thermogravimetry, X-ray diffraction and transmission electron microscopy. *Microporous Mesoporous Mater.* **2001**, *48*, 127–134. [CrossRef]

26. Martinez, D.S.T.; Paula, A.J.; Fonseca, L.C.; Luna, L.A.V.; Silveira, C.P.; Durán, N.; Alves, O.L. Monitoring the Hemolytic Effect of Mesoporous Silica Nanoparticles after Human Blood Protein Corona Formation. *Eur. J. Inorg. Chem.* **2015**, *2015*, 4595–4602. [CrossRef]
27. Trebinska-Stryjewska, A.; Swiech, O.; Opuchlik, L.J.; Grzybowska, E.A.; Bilewicz, R. Impact of Medium pH on DOX Toxicity toward HeLa and A498 Cell Lines. *ACS Omega* **2020**, *5*, 7979–7986. [CrossRef]
28. Cai, L.; Qin, X.; Xu, Z.; Song, Y.; Jiang, H.; Wu, Y.; Ruan, H.; Chen, J. Comparison of Cytotoxicity Evaluation of Anticancer Drugs between Real-Time Cell Analysis and CCK-8 Method. *ACS Omega* **2019**, *4*, 12036–12042. [CrossRef]
29. Deepa, S.; Kumara Swamy, B.E.; Vasantakumar Pai, K. Voltammetric detection of anticancer drug Doxorubicin at pencil graphite electrode: A voltammetric study. *Sens. Int.* **2020**, *1*, 100033. [CrossRef]
30. Hami, Z.; Rezayat, S.M.; Gilani, K.; Amini, M.; Ghazi-Khansari, M. In-vitro cytotoxicity and combination effects of the docetaxel-conjugated and doxorubicin-conjugated poly(lactic acid)-poly(ethylene glycol)-folate-based polymeric micelles in human ovarian cancer cells. *J. Pharm. Pharmacol.* **2016**, *69*, 151–160. [CrossRef]
31. Gou, K.; Xin, W.; Lv, J.; Ma, Z.; Yang, J.; Zhao, L.; Cheng, Y.; Chen, X.; Zeng, R.; Li, H. A pH-responsive chiral mesoporous silica nanoparticles for delivery of doxorubicin in tumor-targeted therapy. *Colloids Surf. Biointerfaces* **2023**, *221*, 113027. [CrossRef]
32. Zhang, Y.; Ye, Z.; He, R.; Li, Y.; Xiong, B.; Yi, M.; Chen, Y.; Liu, J.; Lu, B. Bovine serum albumin-based and dual-responsive targeted hollow mesoporous silica nanoparticles for breast cancer therapy. *Colloids Surf. Biointerfaces* **2023**, *224*, 113201. [CrossRef]
33. Xu, Y.; Xiao, L.; Chang, Y.; Cao, Y.; Chen, C.; Wang, D. pH and Redox Dual-Responsive MSN-S-S-CS as a Drug Delivery System in Cancer Therapy. *Materials* **2020**, *13*, 1279. [CrossRef]